EEET ECOLOGICAL ENGINEERING & ENVIRONMENTAL TECHNOLOGY

Ecological Engineering & Environmental Technology 2024, 25(2), 70–87
https://doi.org/10.12912/27197050/175785
ISSN 2719–7050, License CC-BY 4.0

Received: 2023.11.19
Accepted: 2023.12.15
Published: 2024.01.01

Intelligent Design of an Ultra-Thin Near-Ideal Multilayer Solar Selective Absorber Using Grey Wolf Optimization Linked to Deep Learning

Oussama Gliti[1*], Mohamed Chafik El Idrissi[2], Mohammed Igouzal[1]

[1] Laboratory of Electronic Systems, Information Processing, Mechanical and Energy, University Ibn Tofail, Kénitra, Morocco

[2] Laboratory of Advanced Systems Engineering, ENSA, Kenitra, Morocco

* Corresponding author's e-mail: oussama.gliti@uit.ac.ma

ABSTRACT

This study explored the development of an optimal effective solar absorber by leveraging recent advancements in artificial intelligence and nanotechnology. A predictive computational approach for designing a multilayer metal-dielectric thin film solar selective absorber, specifically the SiO_2/Cr/SiO_2/Cr/SiO_2/Cu structure was proposed. The adopted approach integrates the transfer matrix method (TMM) as a predictive electromagnetic tool and combines it with the swarm-based heuristic algorithm grey wolf optimization (GWO) linked to machine learning algorithms, specifically the artificial neural network (ANN). Through dynamic modeling and rigorous testing against multiple static versions, the adopted approach demonstrates exceptional predictive performance with an value of 0.999. The results obtained using this novel GWO-ANN approach reveal near-perfect broadband absorption of 0.996534 and low emission of 0.194170594 for the designed thin film structure. These outcomes represent a significant advancement in photo-to-thermal conversion efficiency, particularly for a working temperature of 500 °C and a solar concentration of 100 suns, showcasing its potential for practical applications across various fields. Additionally, the designed structure meets the stringent thermal stability requirements necessary for current Concentrated solar power (CSP) projects. This emphasizes its suitability for integration into existing CSP systems and highlights its potential to contribute to advancements in solar energy technology.

Keywords: nanotechnology, solar selective absorber, multi layer perceptron, grey wolf optimization algorithm, multi layer thin film design, concentrating solar power, deep learning regression, physical vapor deposition.

INTRODUCTION

Addressing the escalating global energy demand while prioritizing environmental preservation is currently a pivotal challenge. Solar power, as a renewable energy source, offers a promising solution by reducing dependence on finite fossil fuels (Ren et al., 2023). With an annual solar influx exceeding 437,850 terawatt-hours, surpassing global energy consumption, and decreasing production costs, solar power emerges as a competitive alternative energy source. In this global transition, Morocco, strategically positioned for solar potential, has embarked on a groundbreaking initiative, the establishment of the world's largest concentrated solar power plant spanning 3,000 hectares (Figure 1). This colossal installation incorporates curved mirrors and an array of movable heliostats, focusing sunlight onto a central receiver at the top of a tower, marking a monumental leap in solar energy infrastructure. This transformative decision positions Morocco at the forefront of solar power generation, shaping the nation as a hub for research and economic viability in the solar energy domain.

Concentrating solar power (CSP) plants, renowned for harnessing high-temperature solar energy, play a pivotal role in transitioning to cleaner and more efficient energy sources. The receiver, responsible for converting concentrated solar energy into heat, is a linchpin in the power generation process. Within the solar-to-thermal

conversion process, solar selective absorbers assume a crucial role. These absorbers intricately capture incident photons within film structures across the solar radiation wavelength range, curbing heat loss by suppressing infrared re-radiation. The effectiveness of these absorbers crucially hinges on two primary criteria: solar absorptance (α) and thermal emittance (ε).

Advancements in achieving highly selective absorbing coatings have birthed multilayer solar selective absorbers. By employing alternating dielectric and metal layers (D-M-D), these designs intensify solar absorption through multiple reflections at layer interfaces. They offer broad solar radiation wavelength range coverage, adaptability to various angles, low thermal emittance, high stability, and flexible fabrication methods compared to conventional designs.

The amalgamation of nanotechnology and artificial intelligence is propelling the development of more efficient and cost-effective solar selective absorbers. Their collaboration significantly enhances energy absorption and minimizes heat loss, furthering the evolution of solar energy technology.

The genetic algorithm (GA) and particle swarm optimization (PSO) are leading algorithms in the design and decision-making process (Gliti et al. 2023). Li Voti (2018) employed a genetic algorithm (GA) to search for optimal thicknesses in transparent conducting oxides and transition-metal nitrides, specifically in ITO/TiN multilayered structures with 6, 8, and 10 layers, aiming to achieve very high absorption. (Cai et al. 2022) also utilized GA in a design approach by adding Fe-MgF2 layers on the Fe substrate, achieving an absorption efficiency exceeding 97.9% in the wavelength range of 400–2000 nm. Recently, researchers have begun integrating machine learning algorithms in this field. Seo et al. (2019) computational methods, such as rigorous coupled-wave analysis and the finite-difference time-domain method, are often employed to simulate light-structure interactions in the solar spectrum. However, those methods require heavy computational resources and CPU time. In this study, using a state-of-the-art modeling technique, i.e., deep learning, we demonstrate significant reduction of computational costs during the optimization processes. To minimize the number of samples obtained by actual simulation, only regulated amounts are prepared and used as a data set to train the deep neural network (DNN) employed modeling technique to minimize the computational cost of an optimization process using GA. DNN was employed to construct a robust model capable of predicting solar absorptance for various geometric parameters. By the same approach Ma et al. (2023) utilized a DNN architecture employing the multi-objective double annealing algorithm to discern relationships between parameters of complex nanostructures and optical response spectra, enabling real-time prediction. All these efforts, research endeavors, and predictive capabilities converge towards the common goal of achieving a quasi-perfect solar absorber.

Figure 1. World's largest concentrated solar power plant, Noor Ouarzazate Solar Complex, Morocco (Anouar, 2022))

The conducted research aimed to employ metaheuristic and machine learning algorithms to predict and improve the optical efficiency of solar selective absorbers. Building upon the established multilayer absorber structure (SiO_2/Cr/SiO_2/Cr/SiO_2/Cu) as a reference (Wang et al., 2020; Wu et al., 2021), the study objective was to maximize its thermal photoconversion through the use of the Transfer Matrix Method. To achieve this optimization, two AI algorithms were employed: the Multi-layer Perceptron for predictive dynamic modeling and the grey wolf optimization algorithm to challenge the dominance established by GA and PSO in this field, thereby ensuring a more efficient solar-to-thermal conversion.

DESIGN OF THE MULTILAYER SOLAR SELECTIVE ABSORBER

In the pursuit of achieving the ideal multilayer solar selective absorber, a method involving the alternate arrangement of dielectric and semi-transparent metal layers was employed. This arrangement triggers the occurrence of plasmon resonance and the Fabry-Perot (F-P) cavity (Cai et al. 2022), a fundamental optical phenomenon where light becomes trapped and resonates between two parallel reflective surfaces, as it is shown in Figure 2.

F-P resonators serve to amplify and select particular wavelengths of light, with the resonant wavelengths determined by the spacing and reflectivity of the mirrors. Additionally, surface plasmons, which are collective oscillations of electrons at the surface of a metal, play a significant role in this investigation.

The lower metal layer in a solar absorber serves two purposes: it acts as a reflector to redirect infrared radiation emitted by the heated substrate, reducing the thermal emittance of the absorber, and it minimizes the transmittance of light. The semi-transparent metal layer in the absorber enhances the absorption of incident solar light through multiple reflections with the reflective metal layer, known as the destructive interference effect. The thickness of the semi-transparent layer typically ranges from a few nanometers to around twenty nanometers, depending on the optical properties of the thin metal layer. These semi-transparent metal layers are very thin, typically less than 5 nm, and additional layers can expand the range of wavelengths that are highly absorbed.

Figure 3 displays the materials comprising the studied multi-film, optimized for maximum photothermal efficiency. A copper (Cu) layer was chosen at the bottom, with a thickness exceeding 100 nm, ensuring zero light transmission in the film structure. Silicon dioxide (SiO_2) serves as the selected dielectric material. The initial SiO_2 layer functions as both an anti-reflection and protective layer. The second and third SiO_2 layers serve as phase-matching layers, enabling a second resonance for higher wavelengths. Chromium (Cr), a resonating metal, is well-suited as the absorption layer within the multilayered structure due to its optimal match with the ideal optical properties of the absorption metal, supporting plasmonic resonance in the visible spectrum. Its higher melting point renders it less chemically reactive and comparatively stable for operation in elevated temperature conditions. Studies suggest that the optical constants of Cr depend on thickness (Wang et al., 2020), necessitating specific measurements in thin film rather than bulk material in advance.

The aim of our current research is to theoretically design a 6-layered metal-dielectric

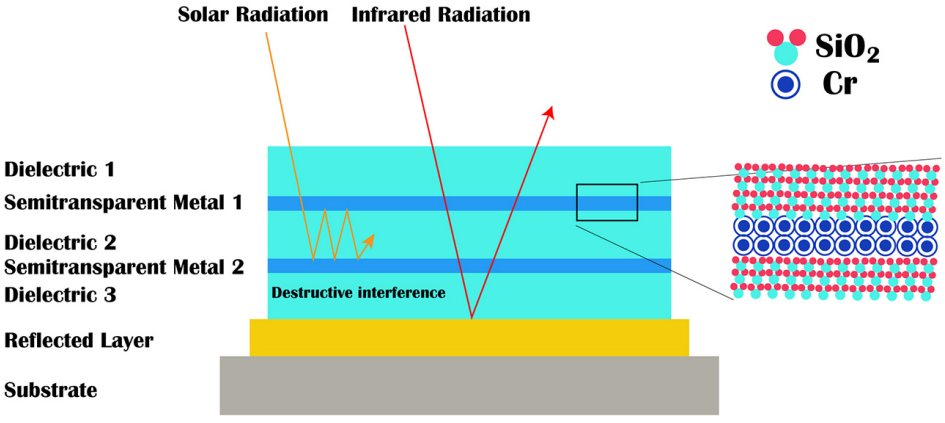

Figure 2. Schematic diagram of the designed six-layered SiO_2/Cr solar selective absorber

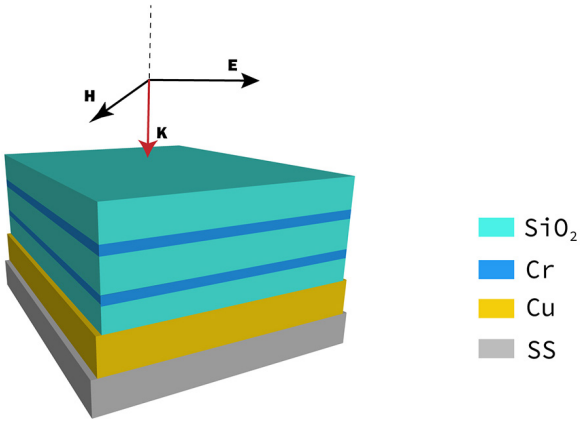

Figure 3. Schematic of the designed absorber with the selected candidate materials

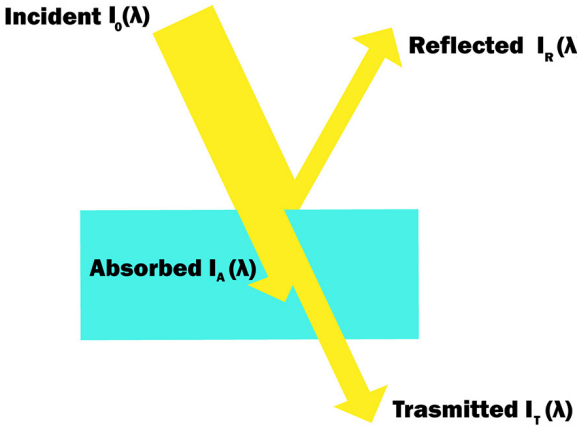

Figure 4. Three phenomena achieved when light interacts with matter, reflection, absorption and transmission of a light beam

multilayered film structure ($Cu/SiO_2/Cr/SiO_2/Cr/SiO_2$) as a selective solar absorber. We aim to enhance its photothermal efficiency by adjusting the thickness values, striving to approach an ideal scenario. The transfer matrix method (TMM) is employed for this purpose.

While particle-swarm optimization and genetic algorithms have traditionally dominated the direct optimization of power conversion for solar selective absorbers, our study introduces a novel approach. For the first time, we will utilize a potent swarm-based algorithm known as the grey wolf algorithm. Combining this with neural networks, the purpose of this work is to precisely determine and predict the ideal configuration.

Spectrally selective coating architecture

Within the domain of physical optics, absorption refers to the process by which a material assimilates incident light or electromagnetic radiation, resulting in the conversion of the energy carried by photons into other forms, primarily thermal energy. It is important to note that absorption does not imply the complete annihilation of light energy; rather, it involves the transfer of energy from the incident photons to the electrons or molecules present within the absorbing material. The interaction between electromagnetic radiation and a material is quantified by its intrinsic parameters. The amount of light reflected (R) and transmitted (T) is determined by the material properties (Figure 4). Conservation of energy dictates that the sum of transmission, reflection, and absorption for each wavelength equals unity as illustrated in Figure 4.

$$R(\lambda) + T(\lambda) + A(\lambda) = 1 \quad (1)$$

An ideal selective solar absorber requires high absorption within the 250–2500 nm solar radiation range while maintaining low absorption and high reflection beyond 2500 nm. This demands 100% absorption/emittance in the shorter wavelength region and zero absorbance/emittance in the longer wavelengths, separated by a distinct transition at the wavelength λ_c. The red curve in Figure 5 represents the ideal case, clearly indicating an abrupt transition at λ_c = 2500 nm from minimal reflection at 0% to a maximum reflection of 100%. As expressed in Equation 2, the goal is to transition sharply from full absorption to zero at this wavelength, ensuring radiative loss remains below the incident solar irradiance. Additionally, it should demonstrate 100% absorption in the solar spectrum, being omnidirectional and polarization-independent, while exhibiting minimal to zero emissivity in the blackbody radiation spectral window, as shown in Figure 5.

$$\begin{cases} \alpha_{max} : R(\lambda) = 0 \text{ for } 0.3 < \lambda < \lambda_c \text{ μm} \\ \varepsilon_{T,max} : R(\lambda) = 1 \text{ for } \lambda_c < \lambda < 50 \text{ μm} \end{cases} \quad (2)$$

Optical performance

To evaluate a solar selective absorber's performance, the solar absorptance ($\alpha(\lambda,\theta)$) is crucial, indicating the ratio of absorbed solar flux density over what the absorber receives from the Sun. Calculations rely on the ASTM G173-03 Direct and Circumsolar (DC) AM1.5 spectrum, covering 300 to 2500 nm at 5 nm intervals. The absorbed solar flux density is derived from the absorptance ($\alpha(\lambda) = 1 - R(\lambda)$) for opaque systems, integrated over the solar spectrum $I_S(\lambda)$.

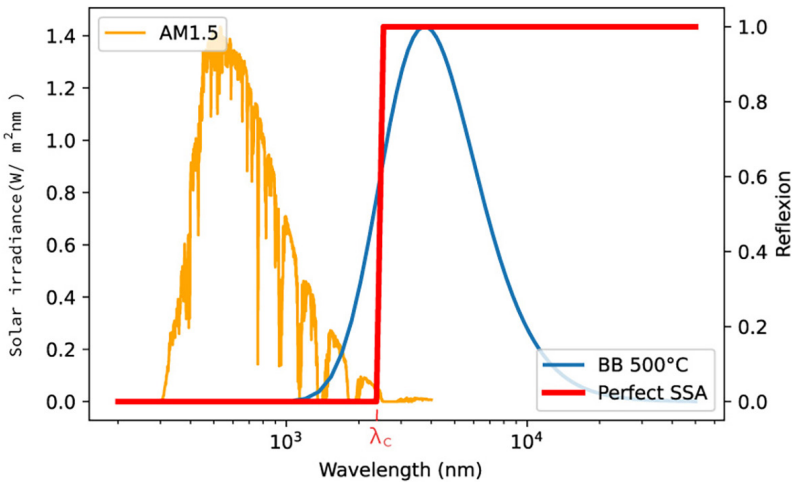

Figure 5. Spectral reflectance of an idealized solar selective coating with the critical wavelength (λ_c). The solar spectral irradiance (ASTM-G173-03) and the normalized blackbody radiation spectrum at 500 °C

$$\alpha(\theta) = \frac{\int_{0.3\mu m}^{2.5}(1 - R(\theta,\lambda))I_s(\lambda)\,d\lambda}{\int_{0.3\mu m}^{2.5} I_s(\lambda)\,d\lambda} \quad (3)$$

Moreover, the effectiveness of the coating is tied to its thermal radiation emission, quantified by its thermal emittance ($I_b(T_A)$). This is the ratio of the emitted irradiance at the absorber's temperature (T_A) to the irradiance of an ideal blackbody at the same temperature. Calculations consider a broad spectral range for accuracy (Grosjean, Soum-Glaude, and Thomas 2021).

$$\varepsilon(\theta, T) = \frac{\int_{2.5\mu m}^{25\mu m}(1 - R(\theta,\lambda))I_b(\lambda, T)\,d\lambda}{\int_{2.5\mu m}^{25\mu m} I_b(\lambda, T)\,d\lambda} \quad (4)$$

$$I_b(\lambda, T_A) = \frac{2\pi hc^2}{\lambda^5 e^{hc/(\lambda k T_a)} - 1} \quad (5)$$

Using Planck's law at temperature T_a (equation 5), the total irradiance emitted by the blackbody is integrated over wavelength (denominator in the equation). Comparatively, the total irradiance emitted by the absorber at T_a (numerator) is calculated by integrating its spectral emittance ($E(\lambda) = 1 - R(\lambda)$) weighted by the blackbody spectral irradiance at T_a, extending from 2500 nm to 50 μm for precise computations.

$$\eta_{solar-th} = \alpha(\theta) - \varepsilon(\theta, T)\frac{\sigma({T_a}^4 - {T_0}^4)}{CI_s\eta_{opt}} \quad (6)$$

The figure of merit (FOM) employed for photo-thermal conversion efficiency assesses the absorber's ability to convert incident solar radiation into heat. It is calculated as the ratio of absorbed solar flux density minus radiative thermal losses, divided by the total concentrated solar flux density received by the absorber (as represented by the equation 6). The variables in these equations, σ, T_a and C, and correspond to the Stefan–Boltzmann constant, operating temperature, solar concentration, and solar flux intensity, respectively. The parameter B, associated with the transmittance of the glass envelope, is typically set to 0.99.

For instance, in this study, the conditions were an operating temperature T_a of 500 °C, a solar concentration of 100 suns, and a solar flux intensity of 1000 W/m² (approximately for ASTM-G173 DC). The heliothermal efficiency indicates the suitability of a coating for high-temperature solar thermal conversion ($T_a >> T_0$).

PHYSICAL VAPOR DEPOSITION

Various wet chemical methods, including electrodeposition, electro-less deposition, anodization, and sol-gel techniques, have been investigated for the fabrication of multi-layer solar selective absorbers. However, these methods exhibit lower chemical and thermal stability and raise environmental concerns related to pollution. Consequently, physical vapor deposition (PVD) has emerged as the preferred technology for crafting these absorbers due to its heightened chemical and thermal stability and diminished environmental impact (Panepinto and Snyders 2020).

PVD and chemical vapor deposition (CVD) are widely utilized in the development of solar energy selective absorbers. PVD, a pivotal

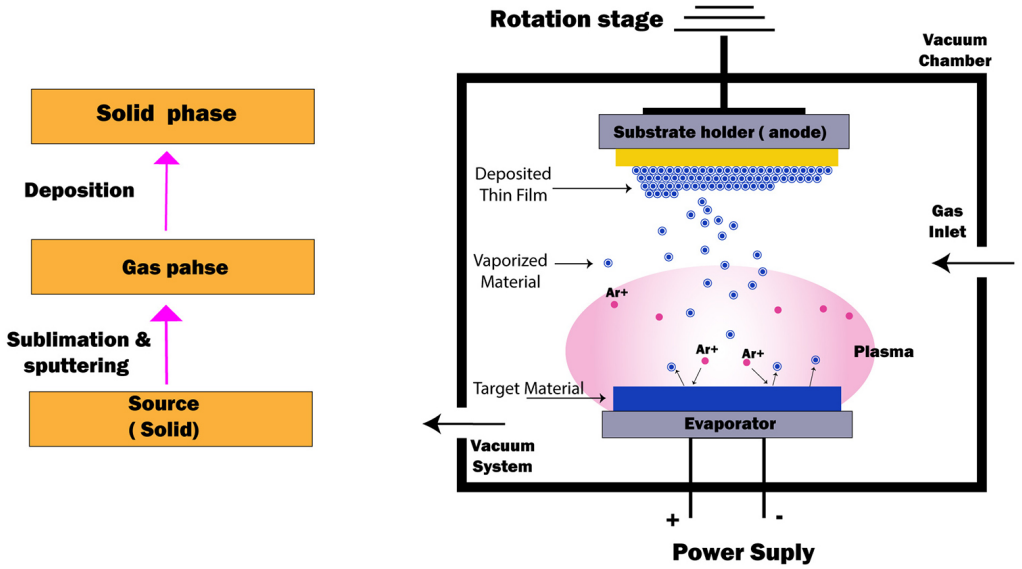

Figure 6. Schematic diagram of physical vapor deposition

tool in nanotechnology, as depicted in Figure 6, involves the vacuum deposition of solid material, which vaporizes and forms a thin film on a substrate. Techniques such as sputtering and thermal evaporation are frequently employed in PVD, enabling precise atom-by-atom deposition and control over the film's density, structure, and atomic composition. Coatings deposited via PVD typically possess thin thicknesses, ranging from atomic layers (less than 10 angstroms (Å) to 0.1 nanometers (nm)) to coatings of several microns. This is achieved through meticulous control of deposition parameters, including deposition rate, temperature, pressure, and substrate properties (Baptista et al., 2018).

ELECTROMAGNETIC CALCULATION

Optical phenomena refer to the interactions between electromagnetic radiation waves and matter. These interactions can be explained using either classical or quantum theories. Maxwell's equations are fundamental in understanding these phenomena and are applicable in both classical and certain semiclassical situations (Zhang et al. 2017).

$$\Delta^2 E = \mu_{diel}\varepsilon_{diel}\frac{\partial^2 E}{\partial t^2} + \mu_{diel}\varepsilon_{diel} \tag{7}$$

$$\mathrm{E} = E_0 \exp\left(\frac{-2\pi k_{ext}}{\lambda}\mathrm{x}\right)\exp\left[i\left(wt - \frac{2\pi n_r x}{\lambda}\right)\right] \tag{8}$$

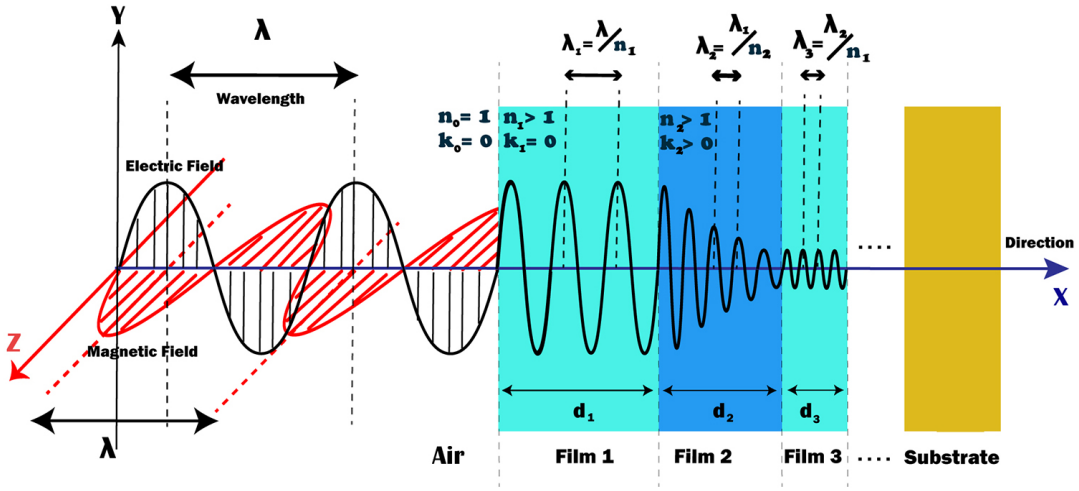

Figure 7. Electromagnetic Light wave travels from air (n = 1; k = 0) into multi film system, transparent film 2 (n = 2; k = 0). and then into the absorbing film 1 (n = 4; k > 0) The phase velocity and wavelength change in each material depending on its complex index of refraction and the thickness of each layer

In the case of solar rays, which are a type of electromagnetic radiation, Maxwell's equations are used to derive their essential physical properties. When dealing with scenarios where there are no free charges and the materials involved are uniform dielectrics, Maxwell's equations specifically describe the electric vector (E) of solar rays.

In this context, the symbols E, μ_{diel}, ε_{diel}, k_{ext}, n_r and λ represent the electric field strength, dielectric permeability, dielectric permittivity, dielectric conductivity, extinction coefficient, refractive index, and wavelength, respectively. On the basis of the one-dimensional solution set, when a solar ray enters a conductive medium (where $\delta_{diel} \neq 0$), it transforms into an evanescent wave. The term $\exp(\frac{-2\pi k_{ext}}{\lambda}x)$ represents the amplitude attenuation, with, k_{ext} indicating the extent of attenuation. Therefore, k_{ext} serves as a measure of the solar energy absorbed by materials. This phenomenon is well illustrated in Figure 7.

As it can also be seen in Figure 7, in optical physics, k_{ext} and n_r serve as fundamental optical constants, playing a vital role in the design of optical film systems (Chen et al., 2019). Solar selective absorbers rely on two primary mechanisms for absorbing incident solar radiation: intrinsic absorption, quantified by the extinction coefficient k, and interference-enhanced absorption, determined by the combination of the refractive index n, film thickness, and substrate properties.

The extinction coefficient k signifies the extent to which a material absorbs light as it traverses through it, offering insights into the absorption characteristics of the material. The refractive index n, a dimensionless value, characterizes how light changes speed or direction upon entering a material from air or vacuum.

The complex refractive index N(λ) = n(λ) + + i k(λ) integrates both the real part (refractive index, n) and the imaginary part (extinction coefficient k), representing how a material interacts with light, accounting for its bending and absorptive properties. This combination allows for a comprehensive description of the interaction of a material with light.

As 1D multilayer structures offer relative simplicity, this research adopted the characteristic matrix method, commonly known as thin-film optics (Sakurai et al. 2014). This method is computationally efficient for modeling the optical traits of such structures. An in-house code, developed using Python, implements this method.

The method assumes isotropic and homogenous mediums within each layer, featuring a spectrally dependent complex relative permittivity. Multilayer absorbers consist of multiple interfaces between different media. Applying boundary conditions for electromagnetic wave propagation at each interface results in the characterization of the q-layer characteristic matrix.

$$\begin{bmatrix} B \\ C \end{bmatrix} = \left\{ \prod_{r=1}^{q} \begin{bmatrix} \cos \Phi_r & \frac{i}{\eta_r} \sin \Phi_r \\ i\eta_r \sin \Phi_r & \cos \Phi_r \end{bmatrix} \right\} \begin{bmatrix} 1 \\ \eta_m \end{bmatrix} \quad (9)$$

where:

$$\Phi_r = \frac{2\pi N_r d_r \cos \theta_r}{\lambda}$$

The variables involved in this calculation include N_r, representing the refractive index of the r-th layer, dr, which stands for the thickness of the r-th layer, Y_r derived from Snell's law, and λ, signifying the wavelength. Notably, this calculation can address the issues associated with solid angle dependence. The optical admittance, denoted as Y_r, is expressed as

$$\begin{aligned} Y_r &= Y_0 N_r \cos\theta_r \text{ for TE wave} \\ Y_r &= \frac{Y_0 N_s}{\cos \theta_s} \text{ for TM wave} \end{aligned} \quad (10)$$

In the context of this study, Y_0 represents the optical admittance within a vacuum or free space. The optical admittance in the substrate, denoted as Y_s, is determined by:

$$\begin{aligned} Y_s &= Y_0 N_s \cos\theta_s \text{ for TE wave} \\ Y_s &= \frac{Y_0 N_r}{\cos \theta_r} \text{ for TM wave} \end{aligned} \quad (11)$$

The calculation of the reflectance in a multilayer absorber involves the solution of Eq. 9. Once the characteristic matrices, denoted as B and C, are obtained through a numerical procedure, the reflectance can be expressed as follows:

$$R = \left(\frac{\eta_0 - Y}{\eta_0 + Y}\right)\left(\frac{\eta_0 - Y}{\eta_0 + Y}\right)^* \quad (12)$$

Then the optical admittance of the single layer can be obtained by $Y = C/B$.

By utilizing the complex conjugate, denoted by *, and setting η_0 = 1, one can theoretically derive the solar absorptance and thermal emittance for diverse optical thin film systems. These outcomes are instrumental in the design and optimization of the optical traits within multilayered solar selective absorbers (Chen, 2021).

The process of fitting reflectance data plays a crucial role in predicting and managing the behavior of materials under different conditions and wavelengths. By accurately representing the behavior of a material through mathematical models, this approach enables the design and advancement of solar absorbers that effectively perform in real-world applications. Fitting reflectance data involves optimizing mathematical models to closely match experimental or measured data, enhancing the understanding of the material properties and refining their characterization.

Duffie and Beckman proposed a calculation method that utilizes measurements of monochromatic reflectance, R(λ), as the available data. By using this data, the spectrum can be easily divided into segments (using the blackbody spectrum for emittance or the incident solar irradiance energy spectrum for absorptance) and perform numerical integration to determine α or ε. Having a grasp of these two-performance metrics enables to establish a benchmark for the developed multilayer thin film, specifically for photothermal applications.

PREDICTION AND OPTIMIZATION

The research objective was to combine a metaheuristic algorithm for optimal solutions with a Machine Learning algorithm for precise predictions. Metaheuristics aim to identify satisfactory solutions for complex optimization problems that are challenging to solve. They specifically address non-linear, non-convex, discontinuous, and discrete optimization problems, especially those that are too large or intricate for traditional methods. Iteratively improving solutions, metaheuristics work to refine problem-solving outcomes. The proposition to the research community emerged subsequent to the publication of the no free lunch (NFL) theorem, which states that no algorithm surpasses all others across all optimization problems. Within the realm of metaheuristic algorithms, swarm-based optimization draws particular inspiration from the collective behavior observed in social animals such as birds, fish, and ants.

On the other hand, regression, a supervised machine learning technique, predicts continuous output based on input features. It establishes a mathematical function or best-fitting line that correlate input variables to the desired output. The primary goal of regression is to find the most accurate model that minimizes the error between predicted and actual target values.

In the considered case, the optical properties of Cr were selected as an illustrative example, sourced from the Palick database (Hu et al. 2017). This data follows a time sequence format, where wavelength acts as the independent variable and (n, k) as the dependent variables for static modeling. The goal was to construct a static model to predict reflection responses for any configuration. Subsequently, fitting these reflection responses through dynamic modeling aids in deriving photothermal conversion, serving as our primary objective.

The curve in Figure 8(a) depicts the optical properties of Cr, showcasing a scatter plot with the red dot representing the Extinction coefficient (k) and the blue dot indicating the refractive index. Notably, fluctuations and non-linearity are apparent in both. In Figure 8(b), a box plot illustrates both optical properties of Cr. Points outside the whiskers may indicate potential outliers, potentially influencing the accuracy of the regression

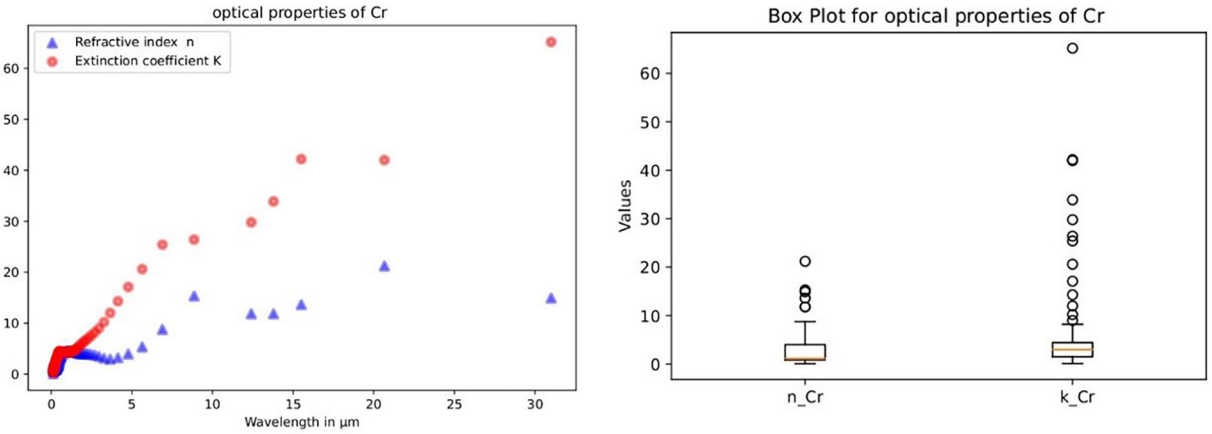

Figure 8. (a) Optical constants refractive index n, and extinction coefficient k of the Cr, (b) Box plot representation of both variables

task. The majority of data is concentrated in the wavelength range 0.2–5 μm, impacting calculations in the infrared.

The necessity for a regression model arises from its capability to address non-linearity, adapt to dynamic modeling with sequentially acquired data, and continuously refine the best predictor for future data. It must be robust against outliers and enable extrapolation beyond experimental values. Once the relationship is established, the regression model can predict values of the dependent variable at unmeasured wavelengths, serving both interpolation and extrapolation purposes. In the considered scenario, extrapolation for the infrared up to 50 μm was utilized. Given the complex non-linear patterns within the data, a highly adaptable model capable of capturing these intricacies is imperative. Neural network regression emerges as a more fitting choice, particularly in handling outliers effectively when appropriately configured. Neural networks offer enhanced suitability for grasping complex patterns and may serve better in managing outliers within the data.

Multi-layer perceptron

The multilayer perceptron (MLP) is an important type of artificial neural network (ANN) that was developed based on neural network models and associated theories, the MLP incorporates variable synaptic weights, which enables it to learn using specific rules. It consists of an input layer, multiple hidden layers, and an output layer as shown in the Figure 9. Each node in the MLP calculates a weighted sum of the inputs, applies a nonlinear activation function, and produces an output. MLPs are widely used in machine learning and pattern recognition because they have the ability to capture complex relationships between inputs and outputs. They can be trained using various algorithms, including backpropagation, which adjusts the network weights to minimize the difference between predicted and actual outputs.

Deep learning presents a marked advantage over traditional machine learning in feature design. In the conventional approach, human effort is heavily involved in crafting features, whereas deep learning diverges by autonomously discerning the most relevant features from raw data, thereby mastering intricate patterns and nonlinear relationships. Neural network regression, adept at capturing complex non-linear patterns within data, becomes the preferred choice when these patterns are intricate and demand a highly adaptable model. Neural networks, particularly multilayer perceptrons (MLPs), excel in capturing non-linearities through their hidden layers non-linear activation functions. These networks possess the ability to approximate nearly any continuous function provided with sufficient data and a fitting architecture, as each neuron contributes to learning simple functions that collectively form more complex ones. This stands in sharp contrast to traditional models where manual feature engineering is a norm for extracting informative features from raw data.

The chosen model comprises fully connected layers whose number and size adapt to the specific problem at hand. These layers are interconnected by rectified linear unit (ReLU) activation functions. Parameter updates are performed using the Adam optimizer, and the loss function is defined as mean squared error (MSE). The input data remains non-standardized, featuring only wavelength values in μm units, reflecting authors'

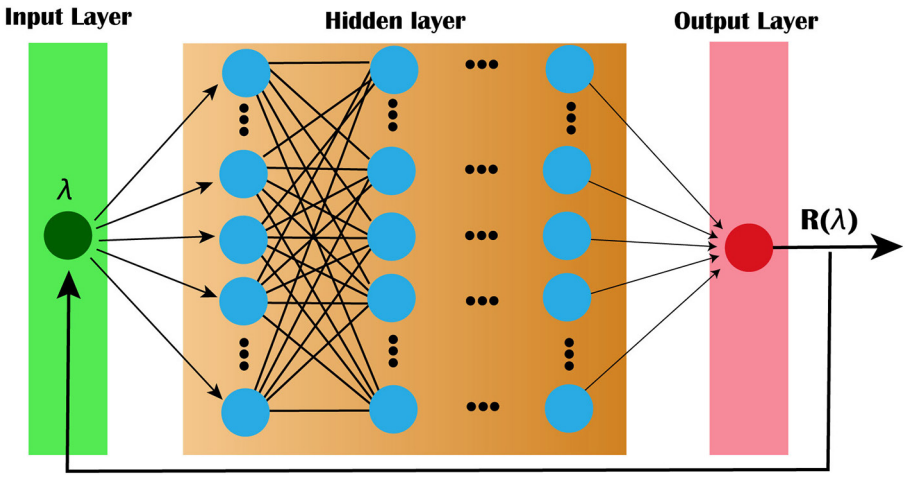

Figure 9. The structure of the nonlinear dynamic autoregressive neural networks

deliberate choice. The entire model was constructed using the Keras tensor flow library in Python. The predictive network consists of five fully connected hidden layers, each with 128, 64, 32, and 16 units, separated by ReLU layers. The training process involves 1000 epochs for each calculation.

Grey wolf optimization algorithm

GWO, a burgeoning swarm intelligence (SI) algorithm, introduced in 2014 by (Mirjalili et al., 2014), draws inspiration from the collaborative hunting behaviors of grey wolves in nature. Differing from PSO, GWO requires less memory as it employs a single vector of position and only retains the three best solutions. This algorithm organizes the population of potential solutions into four hierarchical layers (Figure 10), mirroring distinct roles within a wolf pack. The Alpha wolf symbolizes the best solution found, leading and coordinating the search, while the Beta and Delta wolves represent the second-best and intermediate solutions, respectively, contributing to the exploration-exploitation balance. The Omega wolf, the least dominant, explores extensively, ensuring diversity and preventing premature convergence (Ebrahimi et al., 2023). Through iterative position updates emulating social interactions and hunting behavior, GWO seeks to converge the positions of these wolves toward the optimal solution, advancing the search process.

MATHEMATICAL MODELS OF GWO:

Encircling prey

As previously discussed, the initial phase of the hunting process involves pursuing and surrounding the target as it is shown in Figure 11. In the mathematical model adopted by GWO, two points within an n-dimensional space are considered, and the location of one point is updated based on the position of the other. This simulation is represented by the following equation:

$$X(t+1) = X(t) - A.D \tag{13}$$

Here, $X(t+1)$ represents the subsequent position of the wolf, while $X(t)$ signifies its current location. A stand for a coefficient matrix, and D is a vector determined by the prey's location (X_p), calculated as follows:

$$\mathrm{D} = \left|C.X_p(t) - X(t)\right| \tag{14}$$

where: $C = 2r_2$.

The variable r_2 is derived from a random vector within the range [0, 1]. These equations facilitate the relocation of a solution around another solution. Notably, the utilization of vectors enables the application of these equations across various dimensions. Figure 12 offers an illustration of potential positions of a grey wolf concerning its prey. It is worth noting that the random elements within these equations imitate diverse step sizes and movement velocities of grey wolves. The equations dictating these values are as follows:

$$A = 2a.r_2 - a \tag{15}$$

The elements of vector $\vec{a}$ diminish linearly from two to zero as the iterations progress.

Hunt

The introduced equations grant a wolf the ability to move within a hypersphere surrounding the prey. Nonetheless, these equations alone do not fully encapsulate the social intelligence of grey wolves. As emphasized earlier, social hierarchy significantly influences hunting strategies and

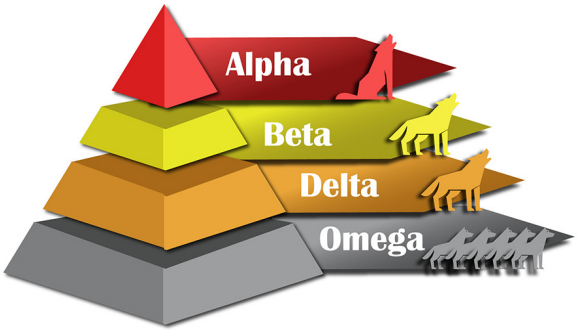

Figure 10. The social structure of grey wolves, dominance decreases progressively from the highest rank downwards

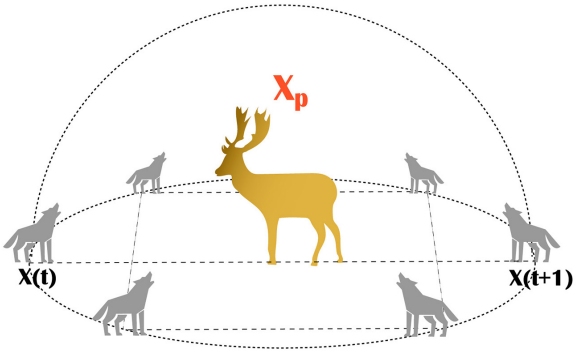

Figure 11. Schematic representation of the encirclement of the prey by the wolves

the survival of wolf packs. To replicate this hierarchy within the GWO framework, three optimal solutions are designated as alpha, beta, and delta. While nature might have multiple wolves in each category, for simplicity, the GWO method assumes a singular solution belonging to each class.

The concepts of alpha, beta, delta, and omega are depicted in Figure 10, with the primary aim being to discover the minimum within this search landscape. As illustrated in the Figure 12, alpha is the closest solution to the minimum, succeeded by beta and delta. The remaining solutions are classified as omega wolves. Although Figure 12 portrays only one omega wolf, the actual count can be higher.

In the GWO method, it is presumed that alpha, beta, and delta consistently represent the three best solutions obtained thus far. As the global optimum for optimization problems remains unknown, it is hypothesized that alpha, beta, and delta possess a good estimation of its location (Faris et al. 2018). This assumption is founded on their status as the best solutions within the entire population. Consequently, other wolves are mandated to update their positions in the following manner:

$$X(t+1) = \frac{1}{3}X_1 + \frac{1}{3}X_2 + \frac{1}{3}X_2 \tag{16}$$

X1, X2, and X3 are computed using Equation 6.

$$\begin{aligned} X_1 &= X_\alpha(t) - A_1 . D_\alpha , \\ X_2 &= X_\beta(t) - A_2 . D_\beta , \\ X_3 &= X_\delta(t) - A_3 . D_\delta \end{aligned} \tag{17}$$

D_α, D_β and D_α are calculated using Eq:

$$\begin{aligned} D_\alpha &= |C_1 . X_\alpha - X|, \\ D_\beta &= |C_2 . X_\beta - X|, \\ D_\alpha &= |C_3 . X_\delta - X| \end{aligned} \tag{18}$$

Algorithm development

Each initialized wolf is chosen as a search agent, representing a configuration of 6 multilayered selective absorbers. To optimize the system successfully, it is crucial to understand the reflective response of each configuration represented by the search agents. Hence, a deep learning approach was employed, renowned for its inherent flexibility and adaptability. Its capability to adjust parameters during the optimization process, similar to a metaheuristic approach, makes it particularly suitable for dynamic modeling. This adaptability enables the model to continually learn and refine its parameters, adapting to the evolving nature of data in real-time or dynamic scenarios. The capacity of MLP to adapt and optimize its parameters aligns with the changing conditions and diverse complexities often encountered in dynamic systems, combining online or dynamic modeling with the grey wolf optimization (GWO) algorithm. This approach involves adapting the parameters of the MLP model as part of the optimization process.

MLP facilitates the prediction of the reflective response for each agent's parameter configuration, as illustrated in Figure 13. These predictions are guidance in calculating the photothermal conversion. This process iterates in each loop. Neural

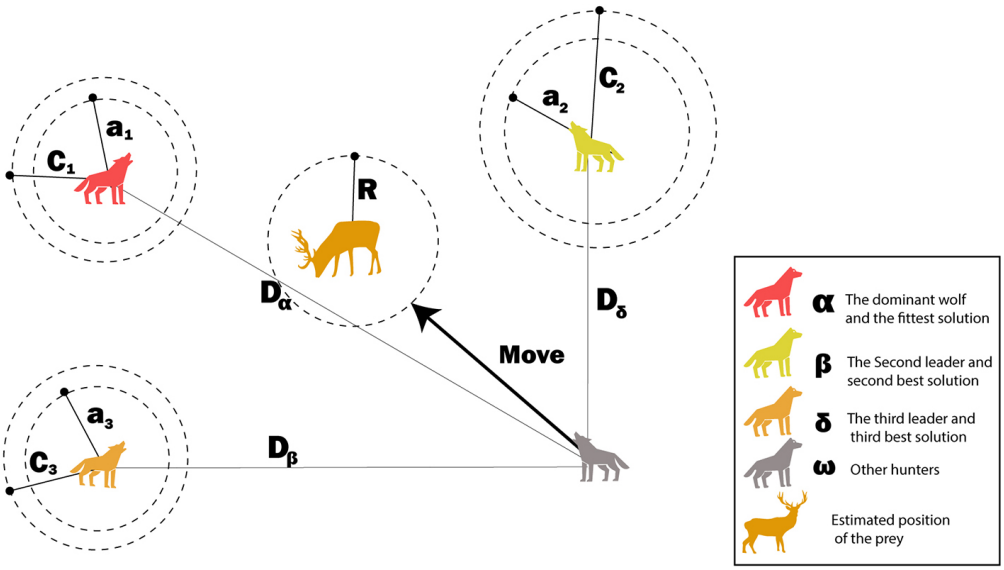

Figure 12. Position updating of the omega wolf, depending on the position of the three leading wolves

networks are often perceived as 'black-box' models or autoregressive nonlinear regressors. While they can model complex relationships, the optimization process is developed with the aid of the Python library MEALPY developed by Van Thieu and Mirjalili (2023).

RESULTS AND DISCUSSION

Boundary conditions of the multilayer SSA

To avoid reaching infinity and achieve logical, manufacturable results, constraints are implemented to ensure that the solutions generated by

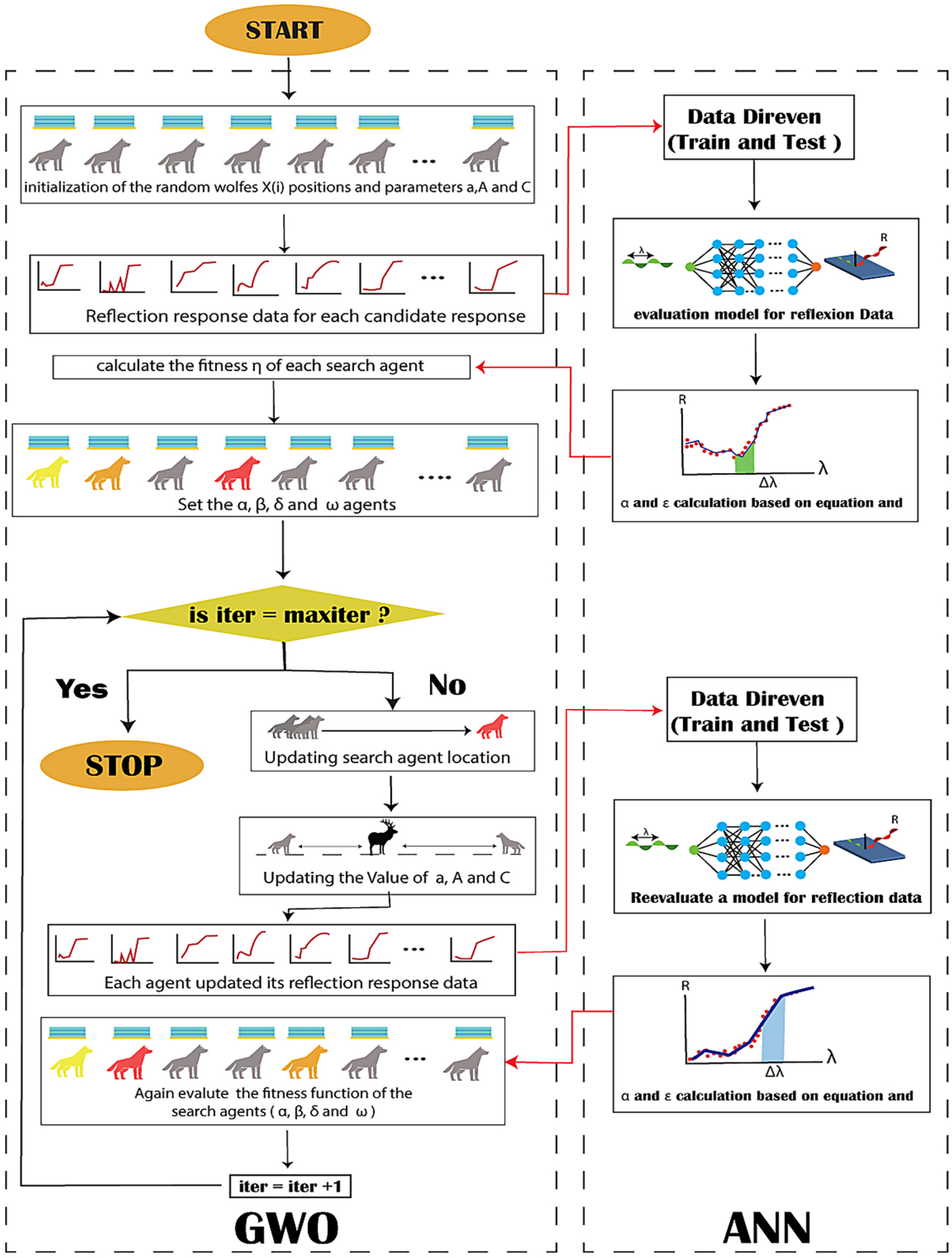

Figure 13. Flowchart of grey wolf optimizer algorithm (GWO) algorithm for optimization linked to artificial neural network (ANN) for dynamic modeling

the metaheuristic algorithm comply with real-world restrictions, including physical or practical limitations. These constraints direct the search towards feasible and practical solutions, conforming to real-world constraints and specific problem requirements.

The advancements in PVD processes, such as molecular beam epitaxy (MBE) and sputtering, have expanded the boundaries of thin film fabrication to sub-nanometer levels. To manufacture ultrathin films, the authors embraced the challenge of significantly reducing the thickness of the Cr absorber layer to 2 nm while maintaining favorable optical characteristics as shown in the Figure 14. The film thickness of the metal absorption layer used in the multilayered solar selective absorber consistently remained below 30.0 nm, which is smaller than its electron means free path. The dielectric layers were confined within a thickness range of 5–100 nm, to create sufficient space for selected light resonance, Table 1 shows the thickness constraint values for each parameter employed in the optimization process.

A group of 20 wolf search agents over 150 iterations was utilized, leading to a cumulative 30,000 calculations throughout the entire process. This encompassed the evaluation of 30,000 models. To optimize the objective function $\eta_{solar\text{-}th}$ and maximize its value, the multilayer was subjected to testing under an irradiance equivalent to 100 suns, maintaining an operating temperature of 500 °C.

Regression metrics

To assess and evaluate the performance of the proposed models along with variations in the configuration, several statistical indices are employed. These metrics offer quantifiable measures of how accurately the model's predictions align with the actual values. Two quantifying accuracy metrics used in this analysis are the Mean Squared Error (MSE) and Mean Absolute Error (MAE), which provide a numerical gauge of the proximity between the model's predictions and the actual values. Lower values of these metrics indicate better performance. Additionally, the R-squared (R^2) metric offers insight into how well the model explains the variance in the data. It is a standardized measure ranging from 0 to 1, where a value closer to 1 indicates superior model performance.

$$\mathrm{MSE} = \frac{1}{n}\sum_{i=1}^{n}(Y_i - \bar{Y}_i)^2 \tag{19}$$

$$\mathrm{MAE} = \frac{1}{n}\sum_{i=1}^{n}|Y_i - \bar{Y}_i| \tag{20}$$

$$R^2 = 1 - \frac{\sum_{i=1}^{n}(Y_i - \hat{Y}_i)^2}{\sum_{i=1}^{n}(Y_i - \bar{Y}_i)^2} \tag{21}$$

where: n – the number of samples;
Y_i – the actual value;
$\hat{Y}_i$ – the predicted value;
$\bar{Y}_i$ – the mean of the actual values.

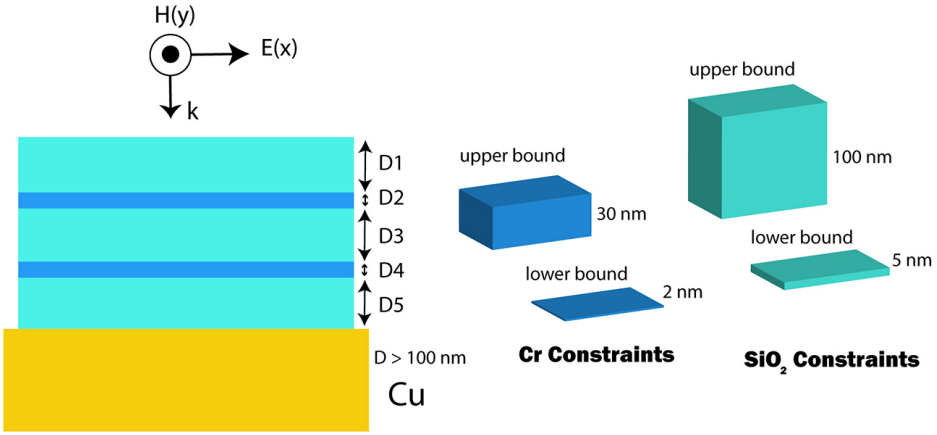

Figure 14. Boundary condition of the metal Cr and the dielectric SiO_2 layers

Table 1. The constraint of each layer thickness in the multilayered thin film absorber

Design parameters	d_1	d_2	d_3	d_4	d_5
Lower bound	5	2	5	2	5
Upper bound	100	30	100	30	100

Static modeling result

For this static modeling, leave-one-out cross-validation (LOOCV) was utilized due to the scarcity of data. LOOCV tends to exhibit lower bias compared to other cross-validation methods because it trains the model on almost all data points. Static modeling involves constructing a model using a fixed dataset without continuous updates or modifications. These models are trained on specific datasets and do not adapt automatically to new incoming data.

A static model that accounts for the variation in optical properties across all wavelengths was employed first. This was achieved by constructing two nonlinear models: the first for the refractive index 'n' and the second for the extinction coefficient 'k.' The effectiveness of the model was a major element in the precise calculation of reflectivity. Once these two values were determined for an entire array of wavelengths, they could be combined to build the complex refractive index. Implementing this complex refractive index into the transfer matrix Method (TMM) formulas enabled to compute the reflection array. This component is crucial and currently missing for a comprehensive understanding of multi-layer performance. As mentioned earlier, for SiO_2, 'n' remains constant across all wavelengths. Similarly, for the substrate Cu, a calculation method similar to that used for Cr was proposed.

From Figure 15, and the regression metrics results already mentioned in Table 2, it can be clearly seen that the model avoids overfitting and perfectly describes the optical reaction to all wavelength variations. Both the refraction and the extinction coefficients for the Cr film increase with the wavelength, showing a metal optical dispersion behavior. Additionally, in the case of extrapolation, the model maintains its increasing nature, which is physically accurate.

Dynamic snapshot ensemble

Online or dynamic modeling involves constructing models that continuously adapt to new data. As mentioned before, the regression modeling task is one part of the optimization loop. In each iteration step, the model receives an update of reflection data with each change in configuration. To assess the accuracy, consistency, adaptability, and performance of the dynamic deep learning model, it was implemented in multiple static versions and compare their outcomes. This process includes creating snapshots of the dynamic model at different time points, treating each snapshot as an independent static model for evaluation.

An illustrative example of the process is shown in Figure 16. Data was randomly selected and shuffle trained based on optimization constraints, choosing six configurations, and evaluating prediction accuracy using regression metrics. The term 'ensemble' is used because

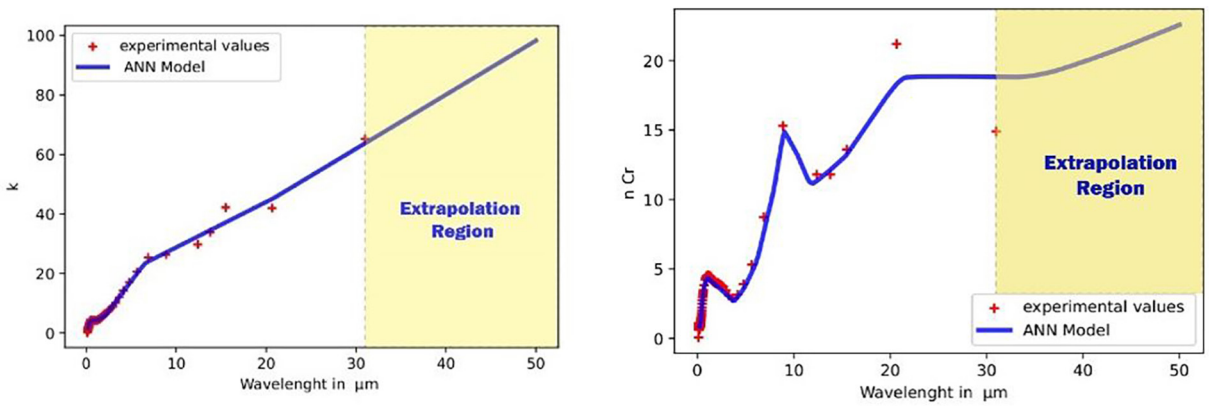

Figure 15. The ANN model predicted on (n,k) test data, and extrapolated over 30 µm

Table 2. Regression metrics score from fitting experimental value refraction and the extinction coefficients for the Cr film

Regression metrics	R^2	MAE	MSE
n (λ)	0.9546	0.227768490853133	0.483468424
K (λ)	0.9953593560375755	0.2068494341174762	0.3892838233448534

it represents a collection of static models, each capturing the dynamic model's state at a specific moment in time. These models collaborate to collectively enhance predictions and adaptability. Each snapshot can be considered a distinct static model, where the model's parameters are frozen at the time of the snapshot. Consequently, each snapshot operates as an independent model without further adaptation.

From the obtained results and the observations in the curves (Figure 17) as well as the results from Table 3, in terms of photothermal conversion and overall optical metrics (such as absorption and emission), the current scenario is

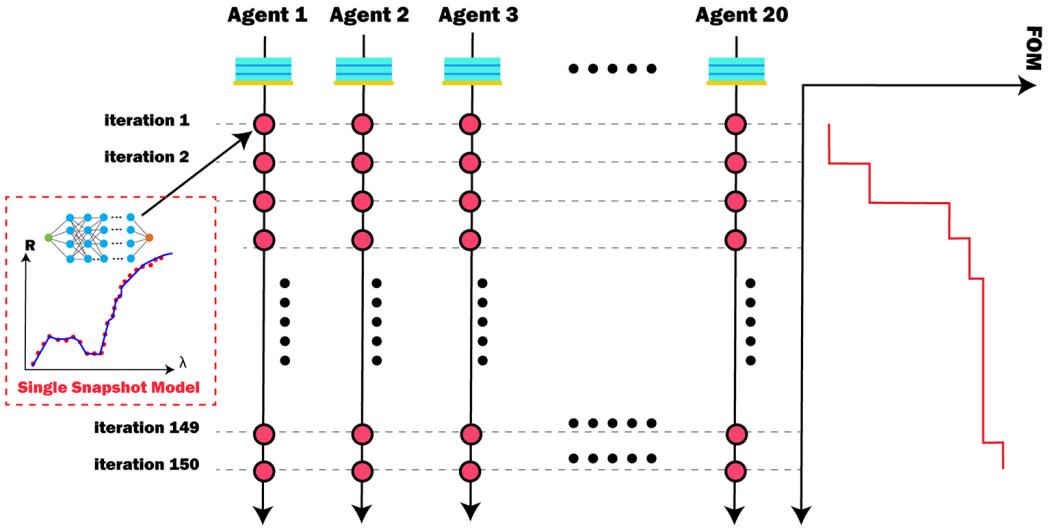

Figure 16. Dynamic modeling for each agent in each iteration

Table 3. Optical performance and regression metric for the 6-configuration shuffled from the constraints

No.	d_1 (nm)	d_2 (nm)	d_3 (nm)	d_4 (nm)	d_5 (nm)	R^2	MAE	MSE	α %	ε (at 500°C)	η (100 sun)
Config1	37.62	23.21	45.30	27.45	14.59	0.9999	0.0006	5.923e-07	0.496	0.14205	0.4605
Config2	84.64	16.98	69.29	6.80	83.68	0.9999	0.00078	1.0106	0.488	0.1555	0.45458
Config3	25.15	3.13	76.96	20.38	98.003	0.99997	0.00057	6.20015e-07	0.486	0.14844	0.52450
Config4	29.62	14.16	77.36	5.61	26.49	0.9999	0.00128	3.8971e-06	0.5482	0.13744	0.5245
Config5	54.16	27.78	64.71	21.87	12.51	0.999	0.00057	9.4893e-07	0.5476	0.1646	0.4759
Config6	95.43	9.903	43.41	25.15	92.67	0.9999	0.00053	5.2470e-07	0.5393	0.1364	0.5055

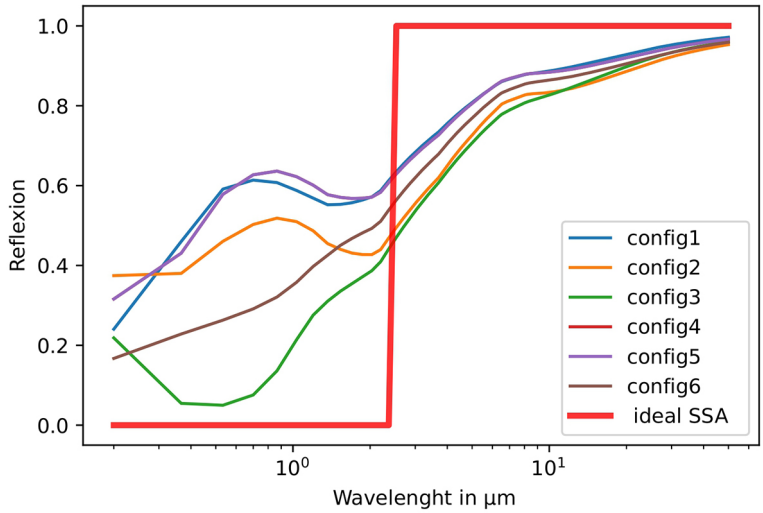

Figure 17. Spectral reflection response curves of the 6-configuration shuffled from the constraints

significantly distant from the ideal situation, the value of the final yield does not reach its maximum. This indicates the necessity for decisions to be made with extreme precision, where even the slightest deviation of a single nanometer is intolerable. the primary interest in this approach lies in the accuracy of prediction. the model's performance across all six configurations, as depicted in the tables, illustrates that the column consistently maintains a favorable predictive value. The same holds for MAE and MSE, which remain as minimal as possible. This reinforces the observation that the model sustains both adaptability and conservatism in its pursuit of accuracy at every stage.

Final optimization result – after completing the optimization process, it is evident that the decisive configuration for enhanced absorption was achieved in the early stages of the hunt (Figure 18), yielding a fitness value of η = 0.959275. The results of the decision parameters and their corresponding absorption and emission values are in Table 4. This optimal configuration consists of SiO_2 (98.0756 nm) / Cr (2.13736 nm) / SiO_2 (71.90734 nm) / Cr (2.83286 nm) / SiO_2 (28.77155 nm) / Cu (>100 nm) and demonstrates broadband near-perfect absorption over the considered range.

Figure 19 shows the reflectance spectra results obtained from the parameters acquired by the GWO-ANN optimization process (Table 4). Clearly, in the visible region, the reflectance spectrum of the simulation remains below 1% for the majority of the solar spectrum, indicating minimal reflection. A slight transition occurs, leading to a maximum absorption of 0.9965%. While introducing additional metal-dielectric stacks could potentially further widen the absorption bandwidth, this would require more effort in manufacturing without significant improvement.

The explanation for the observed resonances lies in the thickness values of each dielectric layer, where net phase shifts, including reflection phases at both top and bottom interfaces, and accumulated propagation in the dielectric layer contribute to thin film interference effects. The reflective properties of metal layers (Cr, Cu) also play a role in selectively absorbing and reflecting incident solar radiation. The spacing between the mirrors and their reflectivity determine resonant wavelengths.

The Fabry-Perot resonance phenomenon occurs when the thickness of the layers in the multilayer structure is a multiple of half the wavelength of the incident light, where m is the mode number). A direct proportionality between these variables is apparent.

It can be concluded that the first layer exhibits a resonance phenomenon at lower wavelengths, while the second layer traps higher wavelengths, especially in the mid-infrared region. According to the results obtained from the GWO-ANN

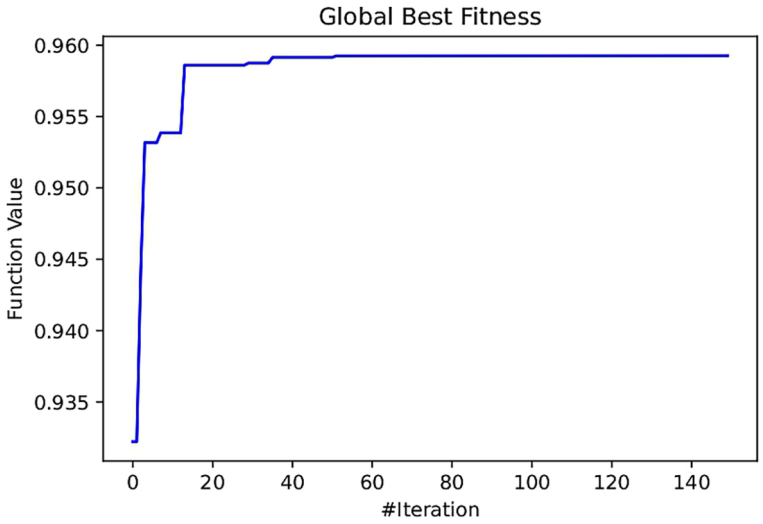

Figure 18. Convergence curve of the six-layered SiO_2/Cr film structure at the working condition of 600 K and 100 Suns

Table 4. Optical performance of the optimized SSA, parameters Recipe For C = 100, Ta = 500 °C

Parameter	d_1	d_2	d_3	d_4	d_5	α	ε (at 500°C)	η (for 100 sun)
GWO linked ANN	98.0756	2.13736	71.90734	2.83286	28.77155	0.996534	0.194170594	0.959275

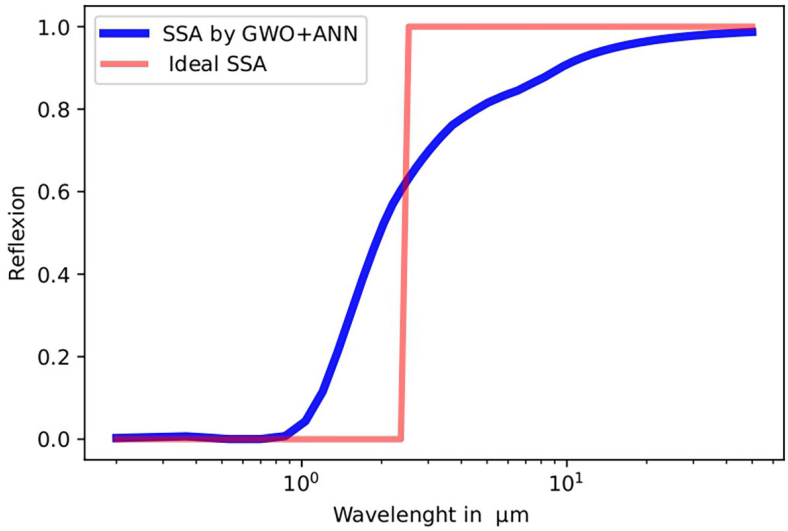

Figure 19. Final result of the reflectance spectra of the designed six-layer solar selective absorber by altering the Cr and SiO_2 layer obtained by the GWO-ANN approach compared to an ideal case

algorithm, the thickness of the dielectric gradually decreases. The combination of these factors leads to constructive interference, enhancing absorption at specific wavelengths

CONCLUSIONS

Exploiting the prediction accuracy and adaptability to feature design inherent in ANN algorithms, this study integrated the ANN into the optimization process of the GWO. This integration served as a competitive alternative to the dominant Algorithms (GA, PSO) in the thin film design field. Leveraging the transfer matrix method tool, we successfully designed a six-layered D-M-D solar selective absorber with the configuration SiO_2 (100 nm) / Cr (2.13736 nm) / SiO_2 (67.0762 nm) / Cr (2.41051 nm) / SiO_2 (30.57438 nm) / Cu (>100 nm). This specific configuration exhibits an impressive absorption value of 0.996534 and an emission of 0.996534, demonstrating near-ideal characteristics. The absorber behaves as a cavity with the right thickness, matching the optimal conditions for resonating the selective solar wavelength through the Fabry-Perot phenomenon.

This result offers a promising prototype for practical implementation using the Physical Vapor Deposition (PVD) method, especially considering the method's capability to achieve minimal thickness values. However, it introduces the challenges associated with manufacturing an ultra-thin film nano Cr layer with a thickness of approximately 2 nm. Additionally, the optical properties of the ultra-thin Cr layer from the bulk exhibit dependence on thickness, given its thickness is smaller than its electron mean free path.

This work aligns with the predictive effectiveness of artificial intelligence algorithms, showcasing their potential in achieving nanotechnological advancements. The goal was to develop a sustainable solution for the photoconversion of solar energy. The increased efficiency derived from the obtained findings translates to a heightened capacity for power generation from available sunlight, enhancing the viability and competitiveness of CSP technologies.

The broad applications across different sectors, including electricity generation, solar desalination, and solar hydrogen production, underscore the versatility and practical implications of the presented research. By addressing challenges and emphasizing practical applications, this study contributes to the ongoing efforts in advancing sustainable solutions for solar energy.

REFERENCES

1. Anouar S., 2022. Morocco has invested $5.2 billion in solar energy projects, https://www.moroccoworldnews.com/2022/08/350593/morocco-has-invested-5-2-billion-in-solar-energy-projects
2. Christofaro B., 2022. Small Morocco punches above its weight on renewables, dw.com,https://www.dw.com/en/morocco-powering-ahead-of-other-african-states-on-renewables/a-64093142

3. Baptista, A., Silva F., Porteiro J., Míguez J., Pinto G. 2018. Sputtering physical vapour deposition (PVD) coatings: A critical review on process improvement and market trend demands. Coatings, 8(11), 402.
4. Cai, H., Wang M., Wu Z., Wang X., Liu J. 2022. Design of multilayer planar film structures for near-perfect absorption in the visible to near-infrared. Optics Express, 30(20), 35219.
5. Chen, H.-P., Lee C.-T., Liao W.-B., et al. 2019. Analysis of high-efficiency mo-based solar selective absorber by admittance locus method. Coatings 9(4): 256.
6. Chen, L.-Y., ed. 2021. Optical properties of solar absorber materials and structures. Topics in Applied Physics, Vol.142. Singapore: Springer Singapore. https://link.springer.com/10.1007/978-981-16-3492-5, accessed October 7, 2023.
7. Ebrahimi, S., Mohammadreza, S.H., Khatibi, S. 2023. Parameter identification of fuel cell using repairable grey wolf optimization algorithm. Applied Soft Computing, 147, 110791.
8. Faris, H., Aljarah, I., Al-Betar M.A., Mirjalili, S. 2018. Grey Wolf Optimizer: A Review of Recent Variants and Applications. Neural Computing and Applications, 30(2), 413–435.
9. Grosjean, A., Soum-Glaude, A., Laurent T. 2021. Influence of Operating Conditions on the Optical Optimization of Solar Selective Absorber Coatings. Solar Energy Materials and Solar Cells, 230, 111280.
10. Hu, E.-T., Guo S., Gu T., et al. 2017. High Efficient and Wide-Angle Solar Absorption with a Multilayered Metal-Dielectric Film Structure. Vacuum, 146, 194–199.
11. Li, V., Roberto. 2018. Optimization of a Perfect Absorber Multilayer Structure by Genetic Algorithms. Journal of the European Optical Society-Rapid Publications, 14(1), 11.
12. Ma, Wenzhuang, Wei Chen, Degui Li, et al. 2023. Deep Learning Empowering Design for Selective Solar Absorber. Nanophotonics 12(18): 3589–3601.
13. Mirjalili, S., Mirjalili S.M., Lewis A. 2014. Grey Wolf Optimizer. Advances in Engineering Software, 69, 46–61.
14. Morocco, with the World's Largest Concentrated Solar Power Plant, among the Leaders in Renewable Energy N.d. Panepinto, A., Snyders, R. 2020. Recent Advances in the Development of Nano-Sculpted Films by Magnetron Sputtering for Energy-Related Applications. Nanomaterials 10(10): 2039.
15. Sakurai, A., Tanikawa, H., Yamada, M. 2014.Computational Design for a Wide-Angle Cermet-Based Solar Selective Absorber for High Temperature Applications. Journal of Quantitative Spectroscopy and Radiative Transfer, 132, 80–89.
16. Seo, J., Jung P.H., Kim, M., et al. 2019. Design of a Broadband Solar Thermal Absorber Using a Deep Neural Network and Experimental Demonstration of Its Performance. Scientific Reports, 9(1), 15028.
17. Ssouaby, S., Naim, H., Tahiri, A., Salmane Bourekkadi, S. 2021. Sensitization Towards Aerosol Optical Properties And Radiative Forcing, Real Case In Morocco. S. Bourekkadi, H. Hami, A. Mokhtari, K. Slimani, and A. Soulaymani, eds. E3S Web of Conferences, 319, 02027.
18. Van Thieu, N., Mirjalili, S. 2023. MEALPY: An Open-Source Library for Latest Meta-Heuristic Algorithms in Python. Journal of Systems Architecture, 139, 102871.
19. Wang, Z.-Y., Hu E.T., Cai Q.Y., et al. 2020. Accurate Design of Solar Selective Absorber Based on Measured Optical Constants of Nano-Thin Cr Film. Coatings, 10(10), 938.
20. Zhang, K., Hao, L., Du, M., et al. 2017. A Review on Thermal Stability and High Temperature Induced Ageing Mechanisms of Solar Absorber Coatings. Renewable and Sustainable Energy Reviews, 67, 1282–1299.